Numerical installation of OE piles in soft rocks within the GPFEM framework

Previtali, Marco; Ciantia, Matteo O.; Riccio, Thomas

Published in:
Proceedings of the 10th European Conference on Numerical Methods in Geotechnical Engineering

DOI:
10.53243/NUMGE2023-322

Publication date:
2023

Document Version
Publisher's PDF, also known as Version of record

Proceedings 10th NUMGE 2023
10th European Conference on Numerical Methods in Geotechnical Engineering
Zdravkovic L, Kontoe S, Taborda DMG, Tsiampousi A (eds)

https://doi.org/10.53243/NUMGE2023-322

Numerical installation of OE piles in soft rocks within the GPFEM framework

M.Previtali[1] , M.O.Ciantia[1] , T.Riccio[1]

[1]*School of Science and Engineering, University of Dundee, Dundee, UK*

ABSTRACT: Pile installation in soft rocks, i.e. chalk, still poses significant design and construction challenges. Episodes of pile run and refusal, both detrimental for the offshore industry continue to occur. This is in part due to the mechanical behaviour of soft-rocks, that in dynamic hydro-mechanical (HM) coupled conditions, become very complicated because of the localised collapse/de-structuration of the initially intact rock. Herein, a constitutive model for soft rocks, calibrated on laboratory data, is implemented within the GPFEM framework and is used to simulate open-ended pile installation in an idealized, homogeneous chalk layer. To prevent mesh dependency during strain localization, a non-local integral regularization is adopted. The results appear to capture the trends observed in the field, such as pile capacity and radial stress profile, showcasing the ability of the GPFEM framework as an useful tool to aid the interpretation of field results and predicting pile capacity.

Keywords: Chalk; Large deformations; Insertion problems in Continuum Mechanics; Coupled H-M

1 INTRODUCTION

The global offshore wind sector has shown a significant growth in the last years, to meet the increasing demand for renewable energy. In this scope, a vast quantity of potential locations for Offshore Wind Farms (OWF) in the North Sea and South Chinese Sea reside over a seabed of high-porosity soft rocks such as chalk. Unfortunately, pile installation in chalk still poses significant design and construction challenges. Current, design practices (i.e. CIRIA C574) originate from a limited number of field tests (Lord et al., 2002) and prescribe an average ultimate shaft resistance (τ_s) between 20 and 120 kPa, depending on chalk density. At times such design constraints may lead to difficulty in the prediction of driving forces, as well conservative estimations of long-term static capacity (Buckley, Jardine, Kontoe, Parker, et al., 2018b).

Dynamic installation of piles generates high stress concentrations combined with excess pore water pressure (PWP) build up in correspondence of pile tip (Staubach & Machacek, 2020), which in turn causes the rock to crush into a soil-like material, i.e. chalk *putty* (Lord et al., 2002). Field tests highlight the formation of a weak annulus of this de-structured material around the pile shaft during driving, inducing very low average shaft resistance values (Wood et al., 2015). The in-service performance depends on the mechanical behaviour of the confining material and the stress acting on the pile. However, the changes in stress state and material fabric after installation are still poorly understood. Recent data (Buckley et al., 2017; Ciavaglia et al., 2017) showed that the apparent average shaft friction increases in time (up to 400%) after End of Driving (EOD). This phenomenon, however, is not encountered with smaller, close ended piles and quasi-static jacked installation (Buckley et al., 2017; Buckley et al., 2018a). Empirical approaches have been proposed to correlate cone resistance q_t, obtained from standard CPT tests, and chalk resistance to driving, based on the ICP-05 approach (Buckley et al., 2020, 2021; Jardine et al., 2023).

While numerical approaches to mitigate mesh-distortion issues in continuum mechanics have been available for a relatively long time, only in recent years the advances in computational power and numerical modelling allowed their application for large-scale pile installation problems. Notable examples include the Coupled Eulerian-Lagrangian (CEL) method (Staubach & Machacek, 2020), Arbitrary Lagrangian-Eulerian (ALE) (Yang et al., 2020), Material Point Method (MPM) (Martinelli & Galavi, 2021), Smoothed Particle Hydrodynamics (SPH)(Cyril et al., 2019) and the Particle Finite Element Method (PFEM) (Monforte et al., 2018; Ciantia, 2022; Ciantia & Previtali, 2023). Herein, the Particle Finite Element Method (PFEM) is used to simulate the installation and post-setup axial testing of open-ended piles in soft rocks under partially (PD) and fully drained (FD) conditions. Results are compared to field data obtained at the Wikinger (WK) OWF site.

2 MODEL DESCRIPTION

2.1 Numerical Formulation

The PFEM approach uses the classic finite element method to solve the governing equations, coupled with continuous remeshing to overcome mesh distortion issues. The interface between different materials is identified through the alpha-shape approach (Kirkpatrick & Seidel, 1983), while mass balance is maintained through residual-based stabilization (Oñate et al., 2014). The G-PFEM platform used here is an open-source implementation of the method, which focuses on coupled Hydro-Mechanical constitutive models for soils and rocks (Carbonell et al., 2022). Low-order triangular elements are used to streamline the remeshing process, while the incompressibility issues typical of these element types is mitigated through a stabilised mixed formulation (Monforte et al., 2017). One additional degree of freedom is used to track pore water pressure through a reduced-order Biot formulation (Monforte et al., 2018). Pile-rock contact detection is solved using rigid-walls while the normal and tangential contact forces are solved implicitly (Monforte et al., 2018) through the Penalty method (Huněk, 1993) and Coulomb's Law of Friction, respectively.

2.2 Constitutive relationships

The mechanical behaviour of the chalk is captured through an isotropic hardening plasticity model based on the multiplicative split of the deformation gradient. The Modified Cam Clay (MCC) model is used to describe the yield envelope (Monforte et al., 2019) in the stress invariant space (p', q, θ). Non-local hardening laws are used to mitigate mesh dependency during strain localization. Two hardening variables are defined: p_t represents the REV-scale tensile strength of the material due to cementitious bonds, while p_s is equivalent to pre-consolidation pressure of the unstructured material as in classical critical-state models. The size of the yield surface (p_c^*) depends on both parameters, $p_c^* = p_s + (1 + c)p_t$, with c quantifying the effects of bonds on the compressive strength. Given p_c^* and p_t, a highly collapsible material will have high c and low p_s and vice-versa. To account for the tensile strength and frame the model with an isotropic strain hardening plasticity framework, axis translation is used such that:

$$p^* = p' + p_t \tag{1}$$

The evolution of the hardening variables is controlled by the parameters $\rho_{s,t}$ and $\xi_{s,t}$:

$$\dot{p_s} = \dot{\gamma}\, \rho_s p_s \left(-\hat{V} + \xi_s \hat{D}\right) \tag{2}$$

$$\dot{p_t} = -\dot{\gamma}\, \rho_t p_t \left(\left|\hat{V}\right| + \xi_t \hat{D}\right) \tag{3}$$

Where $\dot{\gamma}$ is the plastic multiplier, $\hat{V} \coloneqq tr(\partial g/\partial \boldsymbol{\tau})$ and $\hat{D} = \sqrt{\frac{2}{3}}\, ||dev(\partial g/\partial \boldsymbol{\tau})||$ are the volumetric and deviatoric plastic strains, respectively. Regardless of the conventions adopted, the negative sign indicates that the macroscopic effect of cementitious bonds decreases with plastic deformation, i.e. softening. As detailed in (Riccio et al., 2023), the model is calibrated solely using indirect tensile, unconfined compressive and soft oedometer compression tests (Table 1).

Table 1. Constitutive model parameters

Parameter	Value	Parameter	Value
$\boldsymbol{e_0}[-]$	*0.83*	$\boldsymbol{p_{s_0}}[\boldsymbol{kPa}]$	*3000*
$\boldsymbol{\rho'}[\boldsymbol{Mgm^{-3}}]$	*1.4*	$\boldsymbol{p_{t_0}}$ *[**kPa**]*	*200*
$\boldsymbol{\rho_w}[\boldsymbol{Mgm^{-3}}]$	*1.0*	$\boldsymbol{\rho_s}[-]$	*19*
$\boldsymbol{E}$ $[\boldsymbol{GPa}]$	*1.0*	$\boldsymbol{\rho_t}[-]$	*15*
$\boldsymbol{\nu}$ *[*$-$*]*	*0.12*	$\boldsymbol{\xi_s}[-]$	*0.0*
$\boldsymbol{M(\theta)_f}$ $[-]$	*0.9*	$\boldsymbol{\xi_t}[-]$	*0.5*
$\boldsymbol{M(\theta)_g}[-]$	*1.25*	$\boldsymbol{k_v}[\boldsymbol{ms^{-1}}]$	*2.55e-7*

2.3 Application

An open-ended pile, parametrically equivalent to those mobilised at the Wikinger OWF site (diameter $D =$ 1.37m, wall thickness $w_t = 40$ mm) (Buckley et al., 2020), is jacked at the constant speed $v = 0.15$ m/s. This value was chosen to obtain partially drained (PD) conditions:

$$V_c = \frac{\lambda \gamma_w v D}{p^*_{\_c}\,(1+e_0) k_v} \tag{4}$$

Considering a chalk compressibility index $\lambda = 0.134$ (Liu et al., 2023), this results in a normalized penetration speed $V_c \simeq 100$ (Randolph & Hope, 2004; Staubach & Machacek, 2020), high enough to ensure driving-like excess PWP accumulation (Buckley et al., 2018a; Jardine et al., 2023; Staubach & Machacek, 2020). The pile is installed to a depth of 2.5 meters before being tested axially. The chalk is considered fully saturated and the initial stress is considered to be the one of an elastic material at geostatic stress ($K_0 = \nu/(1 - \nu)$). Fully Drained (FD) installation is also simulated using coupled H-M but with $V_c \ll 1$. A 2D axisymmetric model is used, with boundary conditions shown Figure 1. The upper boundary has a constant water pressure of zero, i.e., free drainage, and no vertical confinement. Interface friction is assumed to be constant along the pile-chalk interface ($\delta = 0.57 \simeq 30°$). The open-ended pile tip is simplified into a semi-circle to avoid sharp edges given the target element size at the interface ($w_t/8$) and to avoid numerical instabilities (Monforte et al., 2022). Remeshing is carried out at each step to

maintain regular elements, while refinement, down to the minimum element size of $w_t/8$, occurs when the non-local deviatoric plastic strain within a given element exceeds the area of the smallest element. The internal scale length for non-local hardening variables is set to $w_t/4$, to capture small-scale phenomena without inducing mesh dependency effects (Oliynyk et al., 2021).

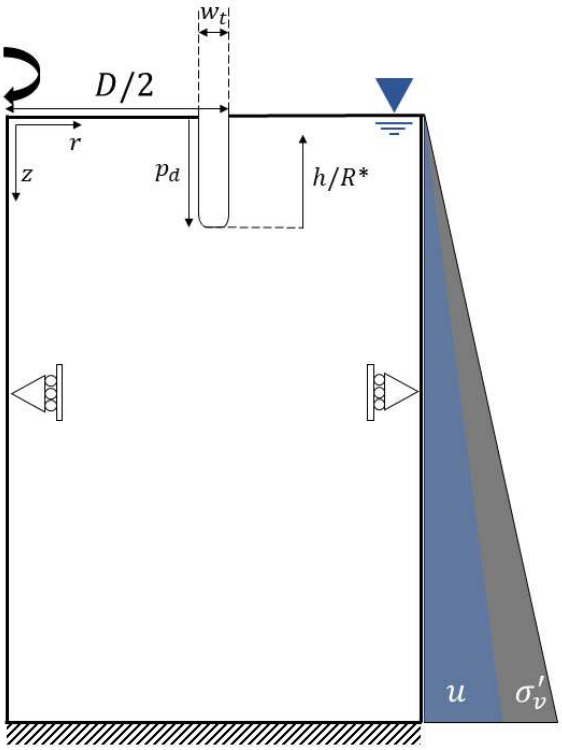

Figure 1: Model geometry and boundary conditions

3 RESULTS AND DISCUSSION

3.1 Pile capacity

The installation force-displacement curves are presented in Figure 2, split between base (Q_b) and shaft (Q_s) capacity. Although the base capacity also increases from partially to fully drained conditions ($\approx 30\%$, Figure 2A), this increment is not as significant as the increment in shaft resistance ($\approx$80%, Figure 2B). Post-installation capacity is computed considering three scenarios after PD installation: (i) no setup, i.e. the pile is tested immediately, (ii) excess pore water pressure (PWP) is dissipated and (iii) pore water pressure is dissipated and chemical reactions (e.g. corrosion) increase the interface friction coefficient δ to 0.84 ($\simeq 40°$). As shown in Table 2, both the tensile and compressive capacity roughly double with the PWP dissipation, reaching the same value obtained during drained installation in the case of compressive capacity. Increasing the interface friction angle by 33% (from 30° to 40°) results in a capacity increase of only $\approx 30\%$. Note that if only the shaft capacity is considered, this value increased by 300% after PWP dissipation and friction increase, close to the values reported in the literature (Buckley et al., 2021). Previous studies in the literature have reported increases in interface friction, albeit only up to 34.5° (Vinck, 2021). Recent research by Jardine et al., (2023) suggests that the increase in shaft capacity is primarily due to an increase in radial stress. This increase in radial stress is the result of a combination of normal dilative displacement of the chalk during interface shearing and expansion of corrosion products.

Table 2: Pile capacity after installation

Total Capacity (MN)	Tensile	Compressive
No setup	-1	9
PWP dissipated	-2	16
PWP dissipated + friction increased	-2.6	20.1

3.2 Radial stress distribution on the pile

The immediately post-installation effective radial stress σ_r' profile has been used in the literature to predict end-of-driving pile capacity based the recorded cone resistance q_t during CPT. The following equation was proposed by (Buckley et al., 2021)

$$\sigma_r' = \zeta q_t \left(\frac{h}{R^*}\right)^{-\eta} \qquad (5)$$

Where h is the distance from the pile tip, normalized by the equivalent pile radius $R^* = \sqrt{R_{out}^2 - R_{in}^2}$. For the piles considered here (WK-OWF), this value is ≈ 0.23 m. The radial stress peaks beneath the tip and decreases exponentially along the pile due to changes in the material fabric caused by the pile movement, i.e. interface shearing. This change in fabric (remoulding) appears to be especially significant for soft rocks (Buckley et al., 2021). The stress distribution along the profile is governed by the parameter η, is a function of pile diameter and wall thickness: $\eta = 0.481(D/w_t)^{0.145} = 0.77$ (Buckley et al., 2021). Finally, the parameter ζ is an empirical fitting factor that correlates the radial stress reduction immediately beneath the CPT cone tip (i.e. q_t) to the stress applied on the shaft (σ_r'), obtained assuming CPT f_s/q_t ratios between 1 and 2% and an interface shear angle of $30.5°$ between the CPT sleeve and the chalk. Here, the radial stress profile obtained from the simulation is normalized using a constant value $q_t = 10MPa$, obtained from numerical CPTs as presented in Riccio et al., (2023). Despite the limited penetration depth reached, the system achieved steady state as evidenced by the stable values of the variables of interest (ie. q_t and PWP). As shown in Figure 3, the numerical data points overlap with those back-calculated from wave equation signal matching (Buckley et al., 2021). The best fitting parameters obtained for (5) appear to slightly underestimate the influence of the h/R^*

relationship, which could be due to the limited penetration depth of these preliminary simulations ($h/R^* \leq 11$) and overlaps almost completely with the one proposed in (Buckley et al., 2020). Note that the model presented here was calibrated on material from St. Nicholas at Wade (SNW), while the tests were carried out on the site of Wikinger OWF. Previous data (Buckley et al., 2018a) indicated that this exponential relationship was present at the SNW site, but no data is available for the test pile model presented here.

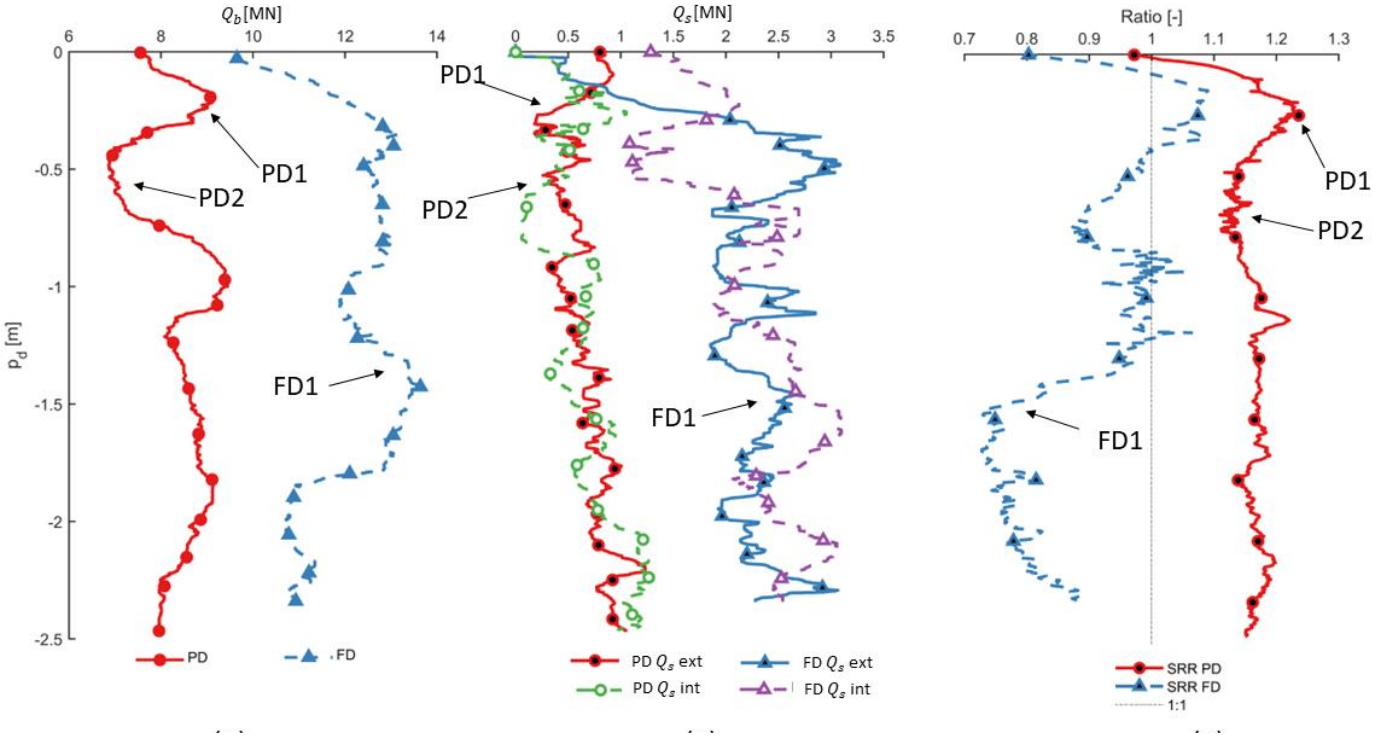

Figure 2: (A) Base and (B) shaft resistance recorded during installation. (C) Specific recovery ratio. The points highlighted by the arrows indicate the invertion in shaft capacity ratios.

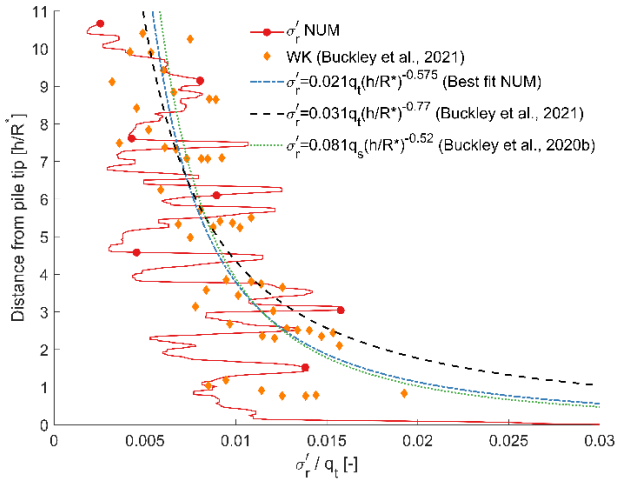

Figure 3: Radial effective stress profile immediately after installation

3.3 Plugging behaviour

The response of the soft rock to pile insertion can be simplified to two ideal cases: (i) coring, in which the material enters the cylinder with minimal damage and internal interface resistance is negligible, and (ii) plugging, in which the material immediately plugs the entrance of the pile and transforms it into a hollow, close-ended structure. This behaviour has been quantified experimentally using the Specific Recovery Ratio (SRR) (Hvorslev, 1949), also known as Incremental Filling Ratio (Zheng et al., 2020), defined as the ratio of change in material cored length to the change in penetration depth. Values of SRR >1 have been recorded in the literature and are typically indices of shear dilation (Monforte et al., 2022). As shown in Figure 2C, the value of SRR is not constant during the installation, despite the constant interface friction parameter prescribed. The authors assume this is due to cycles of friction accumulation at the internal chalk-pile interface, followed by sudden slippage and dilation, which have also been observed experimentally on model piles jacked in chalk (Alvarez-Borges et al., 2018). Specific instants of the simulation in which this occurs are highlighted in Figure 2 (e.g. PD1-2). Calculating the average cross-correlation factor (AVG XCF) between SRR and base/shaft resistance shows significant correlation between increased inner shaft resistance and plugging (Figure 2), anticipated by an increment in tip resistance (LAG ≃ 20 cm), see Table 3.

Table 3 Cross-correlation matrix

Series	$Q_S$int	Q_S ext	Q_b	Q_{tot}
LAG PD [m]	-0.1	-0.1	0.2	-0.2
AVG XCF PD	0.59	0.59	0.6	0.61
LAG FD [m]	0.21	-0.12	-0.21	-0.13

AVG XCF FD	0.58	0.58	0.58	0.55

Surprisingly, the cross-correlation factors obtained for the drained case are similar, despite the more complex material behaviour exhibited by the filling (Figure 4B).

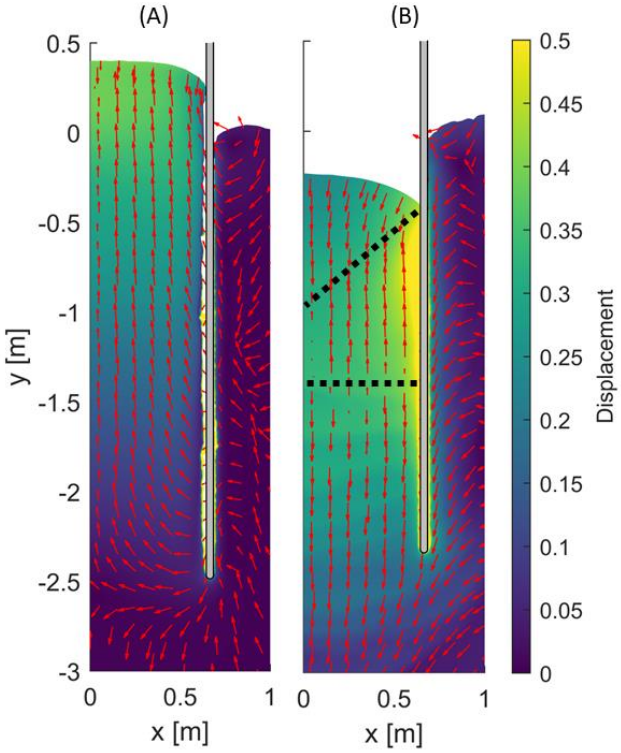

Figure 4: Displacement versors and contour plot for the partially (A) and full (B) drained scenarios. The dashed black lines indicate the invertion in displacement direction.

4 CONCLUSIONS

In this paper, some of the field scale pile tests carried out at the Wikinger OWF site have been reproduced using coupled H-M PFEM simulations. A large strain structured MCC constitutive model is used to describe the behaviour of chalk. Despite the assumptions employed, e.g. homogeneous isotropic intact chalk, the model was able to capture the trends encountered in the field for the limited penetration depth achieved in the simulation. An important result that deviates from the literature is the ratio of internal/external shaft friction, which appears to be much higher than reported ≤ 0.2) and shows significant correlation with the variables that quantify the coring-plugging regimen within the pile. Although pore water dissipation has a noticeable impact on pile capacity, it does not appear to fully account for the increase in capacity observed during pile setup. Recent studies suggested that chemical reactions may play a crucial role in this phenomenon (Jardine et al., 2023). Therefore, future studies should take these factors into account to gain a better understanding of the observed increase in pile capacity during setup.

ACKNOWLEDGEMENTS

This work is an output from the ICE-PICK project, funded by the New Investigator Award EPSRC grant EP/W00013X/1.

5 REFERENCES

Alvarez-Borges, F. J., Richards, D. J., Clayton, C. R. I., & Ahmed, S. I. (2018). Application of X-ray computed tomography to investigate pile penetration mechanisms in chalk. *Engineering in Chalk - Proceedings of the Chalk 2018 Conference*, 565–570.

Buckley, R., Kontoe, S., Jardine, R., Maron, M., Schroeder, F., & Barbosa, P. (2017). Common Pitfalls of Pile Driving Resistance Analysis; A Case Study of the Wikinger Offshore Windfarm. *Offshore Site Investigation Geotechnics 8th International Conference Proceedings*, 1246–1253.

Buckley, R. M., Jardine, R. J., Kontoe, S., Barbosa, P., & Schroeder, F. C. (2020). Full-scale observations of dynamic and static axial responses of offshore piles driven in chalk and tills. *Geotechnique*, *70*(8), 657–681.

Buckley, R. M., Jardine, R. J., Kontoe, S., & Lehane, B. M. (2018a). Effective stress regime around a jacked steel pile during installation ageing and load testing in chalk.

Buckley, R. M., Jardine, R. J., Kontoe, S., Parker, D., & Schroeder, F. C. (2018b). Ageing and cyclic behaviour of axially loaded piles driven in chalk. *Geotechnique*, *68*(2), 146–161.

Buckley, R. M., Kontoe, S., Jardine, R. J., Barbosa, P., & Schroeder, F. C. (2021). Pile driveability in low-to medium-density chalk. *Canadian Geotechnical Journal*, *58*(5), 650–665.

Carbonell, J. M., Monforte, L., Ciantia, M. O., Arroyo, M., & Gens, A. (2022). Geotechnical particle finite element method for modeling of soil-structure interaction under large deformation conditions. *Journal of Rock Mechanics and Geotechnical Engineering*, *14*(3), 967–983.

Ciantia, M. O. (2022). Installation Effects on Axial Performance of Monopiles in Chalk for Offshore Renewables. *Lecture Notes in Civil Engineering*, *208*, 424–432.

Ciantia M.O., & Previtali M. (2023). Finite strain G-PFEM simulation of pile installation in chalk. *Numerical Analysis of Geomaterials*.

Ciavaglia, F., Carey, J., & Diambra, A. (2017). *Monotonic and cyclic lateral load tests on driven piles in chalk*.

Cyril, P. A., Kok, S. T., Song, M. K., Chan, A., Wong, J. Y., & Choong, W. K. (2019). Smooth particle hydrodynamics for the analysis of stresses in soil around Jack-in Pile.

Huněk, I. (1993). On a penalty formulation for contact-impact problems. *Computers & Structures*, *48*(2), 193–203.

Hvorslev, M. J. (1949). *Subsurface exploration and sampling of soils for civil engineering purposes*.

Jardine, R. J., Buckley, R. M., Liu, T., Andolfsson, T., Byrne, B. W., Kontoe, S., McAdam, R. A., Schranz, F., & Vinck, K. (2023). The axial behaviour of piles driven in chalk. *Géotechnique*, 1–45.

Kirkpatrick, D. G., & Seidel, R. (1983). On the Shape of a Set of Points in the Plane. *IEEE Transactions on Information Theory*, *29*(4), 551–559.

Liu, T., Ferreira, P. M. V., Vinck, K., Coop, M. R., Jardine, R. J., & Kontoe, S. (2023). The behaviour of a low- to medium-density chalk under a wide range of pressure conditions. *Soils and Foundations*, *63*(1), 101268.

Lord, J. A., Clayton, C. R. I., Mortimore, R. N., & Construction Industry Research and Information Association. (2002). *Engineering in chalk*. 350.

Martinelli, M., & Galavi, V. (2021). Investigation of the Material Point Method in the simulation of Cone Penetration Tests in dry sand. *Computers and Geotechnics*, *130*, 103923.

Monforte, L., Arroyo, M., Carbonell, J. M., & Gens, A. (2018). Coupled effective stress analysis of insertion problems in geotechnics with the Particle Finite Element Method. *Computers and Geotechnics*, *101*, 114–129.

Monforte, L., Arroyo, M., Carbonell, J. M., & Gens, A. (2022). Large-strain analysis of undrained smooth tube sampling. *Geotechnique*, *72*(1), 61–77.

Monforte, L., Carbonell, J. M., Arroyo, M., & Gens, A. (2017). Performance of mixed formulations for the particle finite element method in soil mechanics problems. *Computational Particle Mechanics*, *4*(3), 269–284.

Monforte, L., Ciantia, M. O., Carbonell, J. M., Arroyo, M., & Gens, A. (2019). A stable mesh-independent approach for numerical modelling of structured soils at large strains. *Computers and Geotechnics*, *116*, 103215.

Muir Wood, A., Mackenzie, B., Burbury, D., Rattley, M., Clayton, C., Mygind, M., Wessel Andersen, K., LeBlanc Thilsted, C., & Albjerg Liingaard, M. (2015). *Design of large diameter monopiles in chalk at Westermost Rough offshore wind farm*.

Oñate, E., Franci, A., & Carbonell, J. M. (2014). Lagrangian formulation for finite element analysis of quasi-incompressible fluids with reduced mass losses. *International Journal for Numerical Methods in Fluids*, *74*(10), 699–731.

Randolph, M., & Hope, S. (2004). *Effect of cone velocity on cone resistance and excess pore pressures*.

Riccio, T., Previtali, M., Ciantia, M., & Brown, M. (2023). The soft-oedometer: a simple test to calibrate advanced constitutive models for CPT simulations in soft rocks. *Convegno Nazionale Dei Ricercatori Di Ingegneria Geotecnica*.

Staubach, P., & Machacek, J. (2020). Impact of the installation on the long-term behavior of offshore wind turbine pile foundations 1. *Soil Dynamics and Earthquake Engineering*, *138*, 106–223.

Vinck, K. (2021). *Advanced geotechnical characterisation to support driven piles design at chalk sites*. Imperial College.

Yang, Z. X., Asce, M., Gao, ; Y Y, Jardine, ; R J, Guo, ; W B, & Wang, D. (2020). Large Deformation Finite-Element Simulation of Displacement-Pile Installation Experiments in Sand. *Journal of Geotechnical and Geoenvironmental Engineering*, *146*(6), 04020044.

Zheng, J. H., Qi, C. G., Zhao, X., Wang, X. Q., & Shan, Y. L. (2020). Experimental Simulation on Open-Ended Pipe Pile Penetration Using Transparent Granule. *KSCE Journal of Civil Engineering*, *24*(8), 2281–2292.